https://doi.org/10.5194/egusphere-2026-6258
Preprint. Discussion started: 3 November 2026
© Author(s) 2026. CC BY 4.0 License.

Channel-morphology-based characterisation and assessment of spatial ice-jam predisposition along the Inner Mongolia reach of the Yellow River

Xinge Shi[1], Honglan Ji[1,2,3], Hongchun Luo[1,2,3], Zhongshu Xue[1], Zijian Chen[1]

[1]State Key Laboratory of Water Engineering Ecology and Environment in Arid Area, Inner Mongolia Agricultural University, Hohhot 010018, China
[2]Inner Mongolia Key Laboratory of Ecohydrology and High Efficient Utilization of Water Resources, Hohhot 010018, China
[3]Inner Mongolia Section of the Yellow River Basin Water Resources and Water Environment Comprehensive Management Autonomous Region Collaborative Innovation Center, Hohhot 010018, China

Correspondence to: honglanji@imau.edu.cn (H. Ji).

Abstract. Ice-jam flood prevention and mitigation remain practical challenges in cold-region river management, making efficient identification of ice-jam-prone reaches essential. Morphology-based assessment can support preliminary screening in data-scarce regions. This study developed a method for assessing spatial ice-jam predisposition along an approximately 800 km reach of the Yellow River in Inner Mongolia. Building on a conventional model, we introduced indicators of shoal development and channel planform complexity, constructed four configurations of the ice-jam predisposition index using different indicator combinations, compared the results at three assessment scales, and examined their spatial correspondence with historical ice-jam records. Predisposition varied markedly, with High-class units concentrated in sections characterised by complex bar-channel configurations and pronounced morphological changes. At the 500 m scale, the full four-indicator configuration classified 11.85% of the units as High; 78.7% of historical records occurred in Medium- or High-class units, and the High-class enrichment ratio reached 2.87. Incorporating shoal development and channel planform complexity improved the differentiation of morphologically complex reaches. The proposed method supports preliminary screening of ice-jam-prone reaches and ice-jam flood management in data-scarce cold-region rivers.

1 Introduction

Ice jams are common river-ice phenomena in cold-region rivers (Hicks, 2009). When moving ice accumulates and obstructs the channel, upstream water levels can rise rapidly and trigger ice-jam floods, threatening levees, riparian communities, and hydraulic infrastructure (Beltaos and Prowse, 2001; IAHR Working Group on River Ice Hydraulics, 1986). The occurrence and evolution of these events depend jointly on discharge, water level, ice conditions, heat exchange, and channel characteristics (Beltaos, 2008; Prowse and Beltaos, 2002). Because these controls interact, ice jams are highly uncertain in both space and time (Lindenschmidt et al., 2019; Madaeni et al., 2020), and their formation locations tend to be strongly site-specific (Arsenault-Boucher et al., 2026). This site specificity complicates both ice-jam identification and ice-jam flood

https://doi.org/10.5194/egusphere-2026-6258
Preprint. Discussion started: 3 November 2026
© Author(s) 2026. CC BY 4.0 License.

management, making the identification of reaches in which moving ice is likely to be arrested and accumulate a central issue in cold-region river-ice research.

Current ice-jam research relies largely on coupled hydrodynamic-thermodynamic models capable of simulating ice-cover evolution, river-ice transport, and ice-jam-induced backwater (Lindenschmidt, 2017; Shen, 2010). Although such models provide a process-based representation, they require continuous observations of hydrological conditions, ice regimes, and channel topography (Kovachis et al., 2017; Lindenschmidt et al., 2024), which restricts their application to long river reaches and data-scarce regions. This limitation has encouraged the development of geospatial approaches based on channel geomorphology. In this context, remote sensing and geographic information systems (GIS) have been used both for ice-jam flood forecasting and for extracting spatial channel information (Gauthier et al., 2008; Unterschultz et al., 2009). Historical ice-jam locations frequently coincide with geomorphic features such as channel constrictions and mid-channel islands (Kalinin, 2008), and GIS-based frameworks have consequently incorporated channel narrowing, sinuosity, and bridges as indicators of river predisposition (De Munck et al., 2017). Related river-ice studies have also highlighted the effects of bridges and confluences on ice transport and jamming (Beltaos et al., 2006; Ettema and Muste, 2001), further demonstrating the relevance of local channel conditions.

The Ningxia–Inner Mongolia reaches of the Yellow River have long faced the risk of ice-jam flooding. Reservoir operation can reduce this risk by changing the flow entering these reaches. However, the benefits depend on how much water the channel can carry and how its shape changes along the river (Su et al., 2019). River bends also affect flow speed and ice movement. These changes can influence how ice cover develops and where ice jams form (Zhao et al., 2021). Channel width, river bends, and the arrangement of bars and channels can therefore help identify places where ice jams are more likely to form. Satellite images show that these features differ along the study reach. Some sections have many shoals or several channels. Other sections have narrow channels. These differences in channel shape can help identify where ice jams are more likely to form.

Existing geospatial assessment frameworks focus primarily on channel constraints and local control features (Arsenault-Boucher et al., 2026). Such indicators describe the overall geometry of the main channel, but narrowing and sinuosity alone may not capture the internal structure of reaches containing well-developed shoals and complex planforms. This limitation is relevant during breakup because the location of ice accumulation depends not only on ice conditions but also on channel hydraulics and local morphology (Beltaos et al., 2003). River-ice processes may, in turn, interact with riverbed erosion, deposition, and morphological adjustment (Ettema and Zabilansky, 2004; Prowse, 2001). To represent this additional source of spatial variability, the present study incorporates both shoal development and channel planform complexity into the predisposition assessment.

Assessment-unit scale determines the spatial extent over which local morphological information is summarised and aggregated (Turner et al., 1989). In reach-based assessments, segment length therefore controls how local characteristics are represented (Frasson et al., 2017; Jelinski and Wu, 1996). Short units retain morphological detail but may produce spatially fragmented results, whereas long units improve longitudinal continuity at the cost of smoothing short-range anomalies (Wu

https://doi.org/10.5194/egusphere-2026-6258
Preprint. Discussion started: 3 November 2026
© Author(s) 2026. CC BY 4.0 License.

et al., 2002). Similar effects have been documented in landslide-susceptibility mapping, where spatial resolution influences both model outputs and their uncertainty (Arnone et al., 2016; Shirzadi et al., 2019), and reviews likewise identify the choice of mapping unit as a key source of variation (Reichenbach et al., 2018). Comparing several segmentation lengths is consequently necessary to determine how strongly the resulting predisposition pattern depends on assessment-unit scale.

Against this background, the study develops a framework for assessing spatial ice-jam predisposition in morphologically complex reaches of the Yellow River in Inner Mongolia. The conventional channel narrowing index (NI) and sinuosity index (SI) are supplemented by a shoal development index (SAI) and a channel planform complexity index (CPCI), which represent shoal abundance and the spatial organisation of the bar-channel structure, respectively. The analysis then addresses three linked questions. First, how is ice-jam predisposition distributed longitudinally when these factors are integrated into a multifactor IJPI? Second, how does the resulting pattern change when assessment-unit length increases from 250 to 500 and 1000 m? Third, do SAI and CPCI provide additional discriminatory information, as indicated by comparisons among model configurations and their spatial correspondence with historical ice-jam records? By answering these questions in sequence, the framework supports preliminary screening, monitoring, and priority-reach management in data-limited cold-region rivers.

2 Study area

The study area covers the Inner Mongolia reach of the Yellow River (Fig. 1) and is about 800 km long. The river flows east along the Hetao Plain and the northern edge of the Ordos Plateau. It then turns southeast towards Wanjiazhai. The study area lies in the arid and semi-arid regions of northern China. The Yinshan Mountains lie to the north, and the Ordos Plateau lies to the south. The river crosses plains, terraces, and areas at the foot of mountains. The terrain and channel shape vary along the reach. Some sections have pronounced bends and local channel narrowing. Other sections have many shoals and multiple channels.

Persistently low winter temperatures cause the river to undergo freeze-up, ice run, and breakup between November and the following March (Wan et al., 2020). Because the river generally flows from lower to higher latitudes, downstream reaches freeze earlier and break up later than upstream reaches (Li et al., 2026). During spring breakup, this longitudinal contrast can produce asynchronous responses among upstream inflow, rising air temperature, and ice transport, thereby favouring local ice accumulation (Prowse et al., 2010). The same setting has repeatedly produced ice jams, ice-induced backwater, and ice-jam flood emergencies, with consequences for flood protection, levee infrastructure, and river management (Fu et al., 2014; Kong et al., 2015). The combination of recurrent events and marked morphological variability therefore makes this reach a representative setting for assessing spatial ice-jam predisposition.

https://doi.org/10.5194/egusphere-2026-6258
Preprint. Discussion started: 3 November 2026
© Author(s) 2026. CC BY 4.0 License.

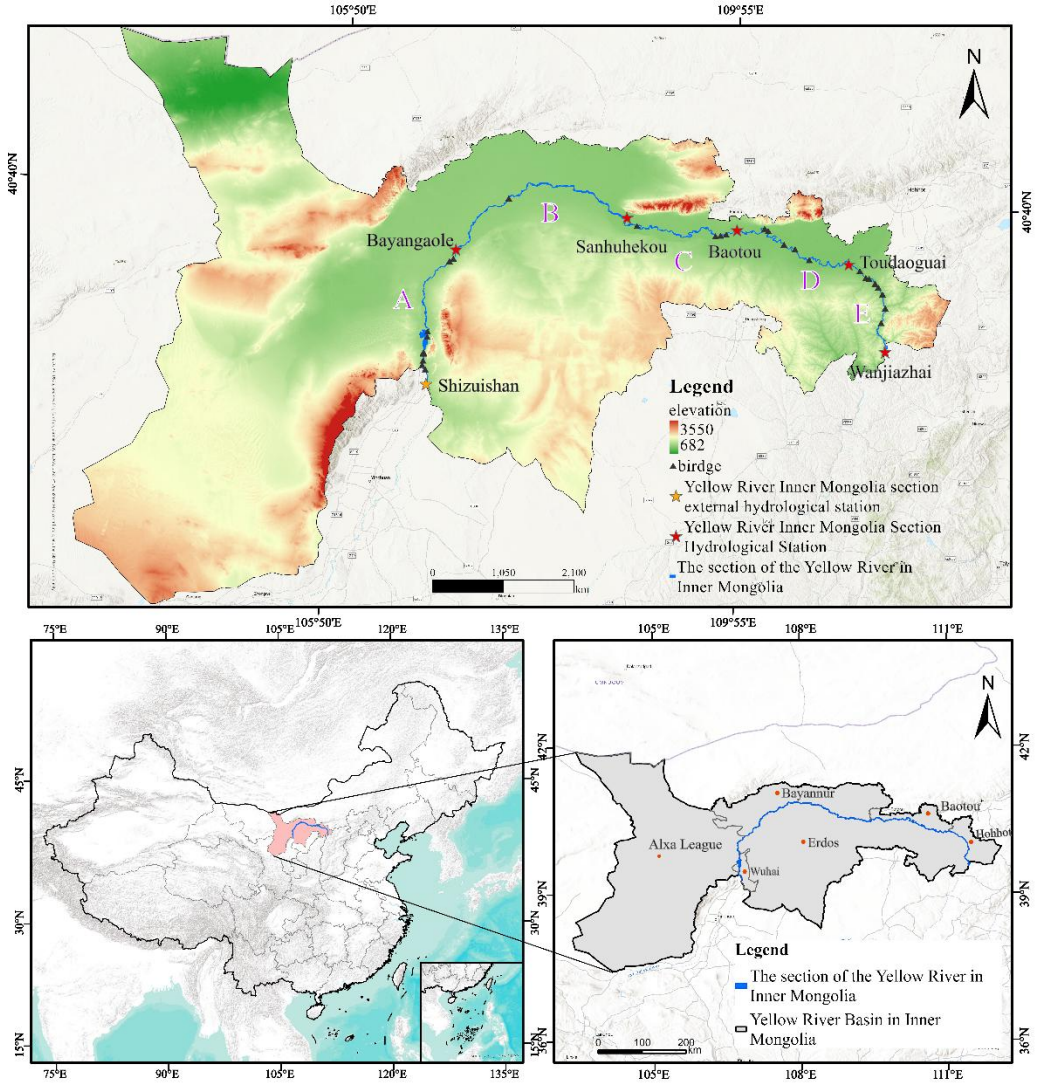


Figure 1. Overview of the study area and delineation of the hydrological control reaches.

3 Materials and methods

3.1 Data sources and preprocessing

Channel morphology was obtained from four HJ-2B satellite images. The images were acquired on 16 and 21 November 2025 and had a spatial resolution of 16 m. Together, they covered the entire Inner Mongolia reach of the Yellow River. Channel and shoal boundaries were identified through manual visual interpretation. The channel boundary marked the extent of the main channel. Shoals were defined as visible bars or shoal areas within this boundary that were not covered by water. Table 1 lists the image dates, data sources, and their uses.

https://doi.org/10.5194/egusphere-2026-6258
Preprint. Discussion started: 3 November 2026
© Author(s) 2026. CC BY 4.0 License.

Historical ice-jam records for 1991-2005 were obtained from Bai et al. (2021), Theory and Practice of Ice-Flood Control Operations in the Ningxia-Inner Mongolia Reach of the Yellow River. Because some records identify only a nearby village, bridge, or river reach, they could not be overlaid directly as precise point locations. Each such event was therefore assigned to the most likely assessment unit by jointly considering place-name locations, upstream-downstream relationships, hydrological control stations, bridges, and other reference information. To keep this interpretation independent of the model results, the IJPI layer was neither displayed nor overlaid during geolocation. The assigned locations were compared with the modelled predisposition classes only after this procedure had been completed. Given the temporal mismatch between the historical records and the 2025 imagery, the comparison was interpreted as a spatial consistency check with the longer-term morphological setting rather than as contemporaneous validation.

Table 1. Data sources and their uses in this study.

Data category	Data source	Period	Quantity	Purpose
Satellite imagery	HJ-2B satellite imagery	16 and 21 November 2025	16 m	Manual delineation of channel and shoal boundaries
Channel morphology data	Manually interpreted from HJ-2B imagery	2025	Based on 16 m imagery	Calculation of centreline, NI, SI, SAI, and CPCI
Historical ice-jam records	Theory and Practice of Ice-Flood Control Operations in the Ningxia–Inner Mongolia Reach of the Yellow River	1991-005	47 records	Historical-record consistency assessment of IJPI results

3.2 Methodological framework

The methodological framework uses relatively stable channel morphology to identify reaches in which moving ice is more likely to be arrested and accumulate (Fig. 2). The main-stem channel was first divided into fixed-length assessment units, after which Channel narrowing index (NI), Channel sinuosity index (SI), Shoal development index (SAI), and Channel planform complexity index (CPCI) were calculated for each unit. These indicators were then converted to ordinal scores and combined under four model configurations. The sequence began with a baseline configuration containing NI and SI; SAI and CPCI were subsequently added to determine how the additional morphological information changed the assessment. The resulting IJPI values were classified as Low, Medium, or High. Finally, the outputs were examined across segmentation scales and indicator combinations and were compared spatially with historical ice-jam records.

https://doi.org/10.5194/egusphere-2026-6258
Preprint. Discussion started: 3 November 2026
© Author(s) 2026. CC BY 4.0 License.

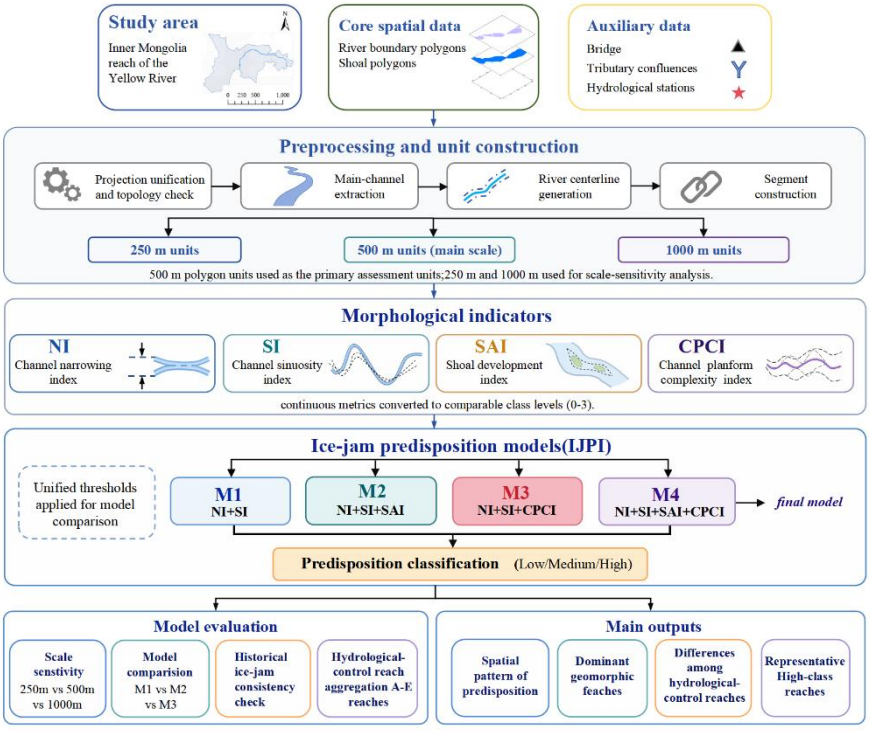


Figure 2. Methodological framework of the study.

3.3 Delineation of river-reach analysis units

To convert the continuous river channel into comparable spatial units, a centreline was extracted from the main-stem channel boundary and divided into fixed-length segments along the flow direction. Each segment was then intersected with the channel boundary to create the assessment unit within which the morphological indicators were calculated. Because the length of these units determines the spatial extent over which morphology is summarised, it can affect both indicator values and the resulting predisposition classification. The analysis therefore used segment lengths of 250, 500, and 1000 m and calculated the IJPI independently at each scale.

To isolate the effect of assessment-unit length, the same indicator calculations and IJPI construction procedure were applied at all three scales. The scale-sensitivity results were then used to select a working scale for the subsequent spatial analyses. Once that scale had been selected, the study area was grouped into five hydrological control reaches (A-E) according to the main hydrological stations, allowing class composition and mean IJPI to be compared longitudinally. This secondary subdivision served only to aggregate and interpret the results; it neither altered the basic assessment units nor entered the IJPI calculation.

https://doi.org/10.5194/egusphere-2026-6258
Preprint. Discussion started: 3 November 2026
© Author(s) 2026. CC BY 4.0 License.

3.4 Channel morphology indicators

Channel morphology constrains ice transport, influences potential retention sites, and can affect the rates of freeze-up and breakup, thereby contributing to spatial variability in river-ice processes (Chu and Lindenschmidt, 2019; Osada et al., 2020). To represent these controls, the assessment uses four indicators: NI, SI, SAI, and CPCI. NI and SI describe changes in channel width and alignment, whereas SAI and CPCI characterise the internal bar-channel structure from complementary perspectives. Specifically, SAI measures the proportion of an assessment unit occupied by shoals and thus represents shoal development, while CPCI incorporates shoal patches, channel boundaries, and their spatial arrangement to describe internal planform complexity. Using the two indices together separates shoal abundance from spatial organisation, which is consistent with the understanding that multiple channels and mid-channel bars jointly shape braided-river planforms (Ashmore, 1991; Murray and Paola, 1994; Williams et al., 2016).

NI describes local channel-width reduction relative to neighbouring upstream reaches. To calculate it, cross-sections were generated at 50 m intervals along the centreline, and the median cross-sectional width was taken as the representative width of each assessment unit. This value was then compared with the maximum effective width within the contiguous upstream sequence, so that the index captured the magnitude of local narrowing rather than absolute channel width alone:

$$NI_i = 1 - \frac{W_i}{W_{up,\max}} \tag{1}$$

Here, W_i is the median channel width of the focal assessment unit, and $W_{up,\max}$ is the maximum effective channel width within the contiguous upstream sequence. Higher NI values indicate stronger local channel narrowing. The channel centreline was sampled at 50 m intervals. Curved reaches were identified from changes in the sign of centreline curvature, with at least 250 m between consecutive inflection points. The sinuosity of each curved reach was defined as follows:

$$SV_j = \frac{L_j}{D_j} \tag{2}$$

Here, L_j is the centreline length of curved reach j, and D_j is the straight-line distance between its endpoints. The sinuosity index was calculated as follows:

$$SV_j = \sqrt{1 - \frac{1}{SV_j^2}} \tag{3}$$

When an assessment unit intersected more than one curved reach, the corresponding SI values were combined using the length of each intersecting reach as the weighting factor. After sinuosity had been assigned in this way, shoal conditions were represented by SAI, which measures the proportion of the assessment unit occupied by shoals:

$$SAI_i = \frac{A_{shoal,i}}{A_{channel,i}} \tag{4}$$

https://doi.org/10.5194/egusphere-2026-6258
Preprint. Discussion started: 3 November 2026
© Author(s) 2026. CC BY 4.0 License.

Here, $A_{shoal,i}$ is the shoal area within assessment unit i, and $A_{channel,i}$ is the area of the corresponding channel assessment unit. SAI therefore represents the areal proportion and degree of shoal development within the unit. SAI represents shoal abundance but does not describe how individual shoals and channel boundaries are organised. CPCI was therefore introduced to capture this additional dimension of planform structure by combining shoal patch density (PD), shoal edge density (ED), and shape complexity (SC). To exclude very small features that could reflect interpretation noise, only shoal patches with an area of at least 100 m² were retained. The three component metrics were calculated as follows:

$$PD_i = \frac{N_i}{A_i} \tag{5}$$

$$ED_i = \frac{\sum_{k=1}^{N_i} P_{ik}}{A_i} \tag{6}$$

$$SC_i = \frac{P_i}{2\sqrt{\pi A_i}} \tag{7}$$

Here, N_i is the number of shoal patches within assessment unit i; P_{ik} is the boundary length of shoal patch k; and A_i and P_i are the area and perimeter of the corresponding channel assessment unit, respectively. To reduce the influence of extreme values, PD, ED, and SC were robustly normalised using the 5th and 95th percentiles as follows:

$$X_i' = clip\left(\frac{X_i - Q_5}{Q_{95} - Q_5}, 0, 1\right) \tag{8}$$

Here, Q_5 and Q_{95} denote the 5th and 95th percentiles of the corresponding metric, respectively. Values below or above this range were truncated to 0 and 1, respectively. The CPCI was then calculated as the equally weighted mean of the three normalised component metrics:

$$CPCI_i = \frac{PD' + ED' + SD'}{3} \tag{9}$$

Here, PD', ED', and SD' denote the three normalised component metrics, respectively.

3.5 Spatial ice-jam predisposition model

The IJPI integrates the morphological conditions associated with the potential retention and accumulation of river ice within each assessment unit. To determine how different types of information affected this representation, four configurations were constructed from different subsets of the classified indicators. The historical ice-jam records were reserved for the subsequent spatial consistency check and did not enter the IJPI calculation. Consequently, differences among the configurations indicate how the inclusion of additional morphological information changes class assignment and the

https://doi.org/10.5194/egusphere-2026-6258
Preprint. Discussion started: 3 November 2026
© Author(s) 2026. CC BY 4.0 License.

identification of highly predisposed reaches; they do not isolate the physical effect of an individual factor during a specific ice-jam event.

Before integration, the continuous indicators were converted to ordinal scores from 0 to 3, thereby placing variables with different units and numerical ranges on a common scale. Within the extended configurations, NI and SI retained the primary weights, while SAI and CPCI supplied information on multi-channel and bar-channel morphology. SAI was assigned a slightly higher a priori weight than CPCI because shoal abundance has a more direct physical connection with ice accumulation, whereas CPCI represents broader planform heterogeneity. This distinction provided the conceptual basis for the baseline weights. Because the weighting scheme was not empirically calibrated, however, its influence was examined separately through alternative weighting scenarios (Saisana et al., 2005).

To ensure comparability among configurations containing different indicator combinations, the IJPI was calculated as a weighted, normalised sum of the ordinal scores. For assessment unit i under model configuration m, the IJPI was calculated as follows:

$$IJPI_i^{(m)} = \frac{1}{3}\sum_{j=1}^{n_m} \omega_j^{(m)} C_{ij}^{(m)} \tag{10}$$

Here, $IJPI_i^{(m)}$ denotes the ice jam predisposition index for assessment unit i under model configuration m. Configuration m is M1, M2, M3, or M4; n_m is the number of morphological indicators in configuration m; $\omega_j^{(m)}$ is the weight assigned to indicator j in configuration m; and $C_{ij}^{(m)}$ is the ordinal score of indicator j for assessment unit j, ranging from 0 to 3. Because the indicator weights sum to 1 and the maximum ordinal score is 3, the weighted sum was divided by 3 so that $IJPI_i^{(m)}$ ranges from 0 to 1. The indicator combinations used in the four configurations are presented in Table 2.

Table 2. Combinations of morphological indicators under the different model configurations.

Model	Indicators
M1	NI, SI
M2	NI, SI, SAI
M3	NI, SI, CPCI
M4	NI, SI, SAI, CPCI

Assessment units were classified as Low (IJPI < 0.45), Medium (0.45 ≤ IJPI < 0.65), or High (IJPI ≥ 0.65). The same thresholds were applied to all four configurations to ensure consistent comparisons. Because the IJPI represents relative predisposition among reaches within the study area, the thresholds were selected from the study-area distribution of IJPI values and denote comparatively low, moderate, and high levels of predisposition. M4 was specified a priori as the full configuration containing all four indicators, whereas M1-M3 served as comparison configurations that omitted one or both newly introduced indicators.

https://doi.org/10.5194/egusphere-2026-6258
Preprint. Discussion started: 3 November 2026
© Author(s) 2026. CC BY 4.0 License.

The assessment was formulated as a conceptual regional model to balance physical-process understanding with applicability along a long, data-scarce river reach. Within this framework, M1-M4 were first compared to determine how the addition of SAI and CPCI changed the spatial representation of predisposition. Weight uncertainty was then evaluated separately using six scenarios based on the full M4 configuration. By varying the relative contributions of the conventional and newly introduced indicators, this analysis examined whether the IJPI ranking, class assignments, and correspondence with historical records remained stable when the assumed weights changed.

3.6 Model evaluation

Model results were evaluated through several comparisons. Scale sensitivity was assessed by comparing results at the 250, 500, and 1000 m scales. The comparison included the mean and standard deviation of IJPI and the proportions of Low, Medium, and High units. Correlations among NI, SI, SAI, and CPCI were calculated to assess information overlap and whether the new indicators added information about channel shape. Agreement across scales was assessed by matching each 250 m unit to the corresponding 500 and 1000 m units. The matching used the distance of each 250 m unit's centre point along the river. A 250 m unit was considered consistently classified as High when all three matched units were in the High class. M1-M4 were also compared to examine how adding SAI and CPCI changed the assessment results.

The historical records provided a separate check on the spatial plausibility of the model outputs. For each configuration, the proportions of records falling within Low-, Medium-, and High-class units were first calculated. Because the positional accuracy and completeness of the records varied, these proportions were interpreted only as measures of spatial consistency. High-class coverage was then complemented by an enrichment ratio, defined as the proportion of historical records in High-class units divided by the proportion of all assessment units classified as High. A value greater than 1 therefore indicates that historical records are over-represented in the High class relative to its prevalence in the study area. To test whether this concentration exceeded random expectation, the 47 historical locations were repeatedly reassigned among the 500 m units while their total number was held constant. The observed High-class coverage and enrichment ratio were then compared with the resulting null distributions using a one-sided empirical p value.

4 Results

4.1 Sensitivity to assessment-unit length

The three segmentation lengths produced similar mean and standard deviation values for IJPI and similar proportions of High-class units (Table 3). At the study-area level, assessment scale therefore had little effect on overall class composition. The locations assigned to the High class, however, changed substantially: the Jaccard indices were 0.112 for the 250-500 m pair, 0.147 for the 500-1000 m pair, and 0.074 for the 250-1000 m pair. Scale selection thus affected the local delineation of highly predisposed reaches more strongly than it affected their overall prevalence.

Table 3. Sensitivity of the IJPI results to assessment-unit length.

https://doi.org/10.5194/egusphere-2026-6258
Preprint. Discussion started: 3 November 2026
© Author(s) 2026. CC BY 4.0 License.

Segment length	Mean IJPI	SD of IJPI	High proportion	Jaccard comparison	Jaccard coefficient
250 m	0.4541	0.1562	11.70%	250 m vs 500 m	0.112
500 m	0.4542	0.1578	11.85%	500 m vs 1000 m	0.147
1000 m	0.4546	0.1541	12.23%	250 m vs 1000 m	0.074

Cross-scale matching clarified which of these local patterns were least sensitive to assessment-unit length. Under M4, 172 individual 250 m units were classified as High at all three scales, representing approximately 43.0 km of channel. These units accounted for 5.48% of all 250 m units and 46.9% of the High-class units at that scale (Fig. 3). Their repeated identification makes them suitable candidates for priority screening, although it does not imply a probability of ice-jam occurrence. For the remaining analyses, 500 m was retained as the working scale because it balanced local morphological detail with longitudinal continuity.

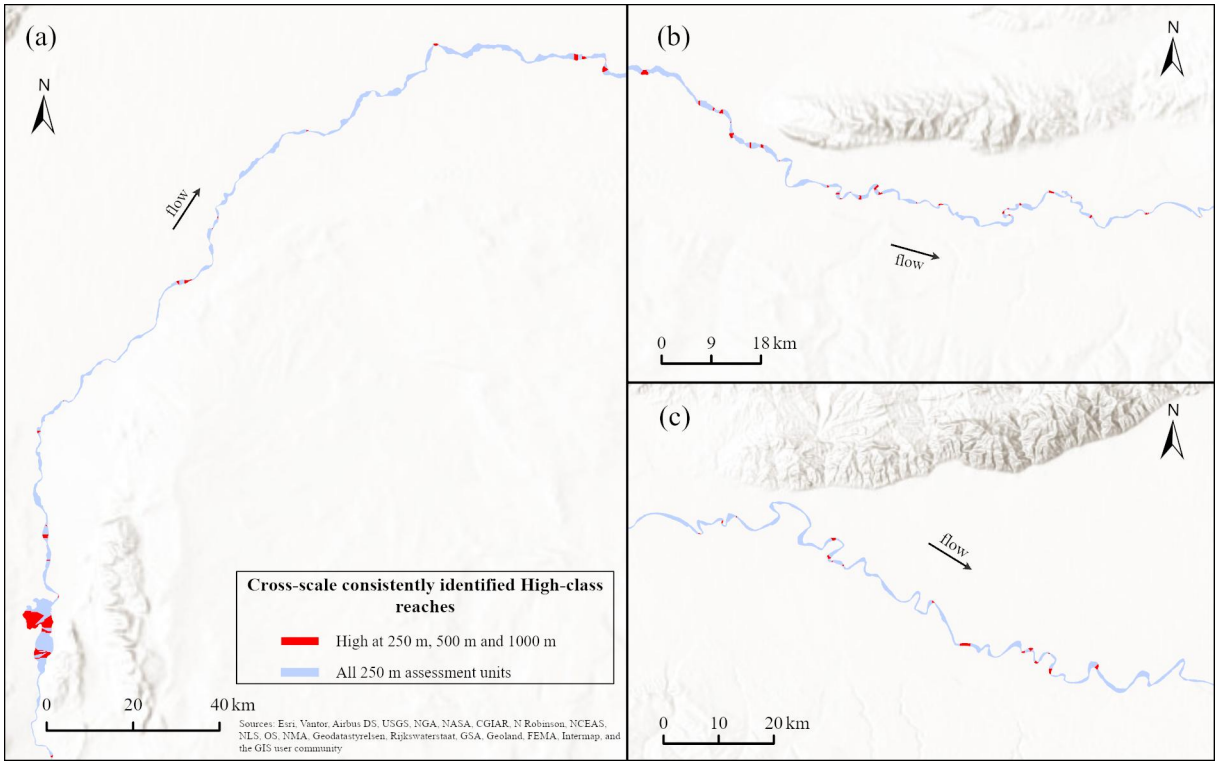


Figure 3. Spatial distribution of reaches consistently classified as High by M4 at assessment-unit lengths of 250, 500, and 1000 m. Panels (a)–(c) show the study reach from upstream to downstream.

4.2 Correlations and class distributions of channel-morphology indicators

The relationship between each morphological indicator and the composite IJPI was broadly consistent across the 250, 500, and 1000 m scales (Fig. 4). SI had the strongest correlation at every scale, with coefficients above 0.85, while CPCI ranked

https://doi.org/10.5194/egusphere-2026-6258
Preprint. Discussion started: 3 November 2026
© Author(s) 2026. CC BY 4.0 License.

second with coefficients of approximately 0.40-0.48. NI and SAI were more weakly correlated with IJPI and showed only small scale-related fluctuations. Although changing segment length therefore altered individual local values, the stable ordering of the correlations indicates that it did not materially change the relative composition of the composite index.

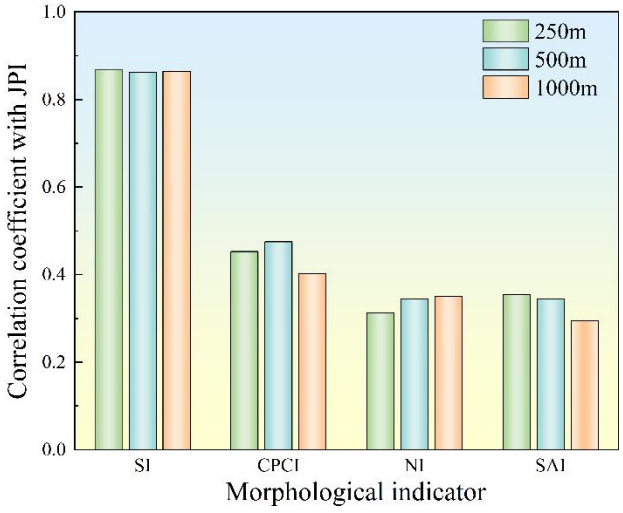


Figure 4. Spearman's rank correlations between the channel-morphology indicators and IJPI at different assessment scales.

The inter-indicator correlations at the 500 m scale show why the four variables contribute different information (Table 4). NI was weakly correlated with SI, SAI, and CPCI (0.030, -0.113, and 0.090, respectively), and SI was similarly weakly correlated with SAI and CPCI (0.027 and 0.089). Channel narrowing, sinuosity, and bar-channel complexity therefore do not generally coincide in space. SAI and CPCI were more strongly correlated ($\rho = 0.739$) because both depend partly on shoal information. Nevertheless, CPCI also incorporates patch density, edge characteristics, and channel planform, so it retains a different emphasis from the areal measure represented by SAI.

Table 4. Spearman's rank-correlation matrix for the ordinal scores of the channel-morphology indicators.

Index	NI	SI	SAI	CPCI
NI	1	0.030	-0.113	0.090
SI	0.030	1	0.027	0.089
SAI	-0.113	0.027	1	0.739
CPCI	0.090	0.089	0.739	1

These differences among the indicators were also reflected in their distributions across the predisposition classes (Fig. 5). Low-class reaches generally combined low indicator scores with relatively simple morphology. From Low to Medium, several indicators increased, most notably SI and CPCI; in the High class, both the mean scores and the ranges of these two indicators increased further. NI and SAI changed less markedly among classes, but they still altered the classification of

https://doi.org/10.5194/egusphere-2026-6258
Preprint. Discussion started: 3 November 2026
© Author(s) 2026. CC BY 4.0 License.

individual reaches when combined with the other variables. The three predisposition classes therefore represent different combinations of morphological conditions rather than thresholds in any single indicator.

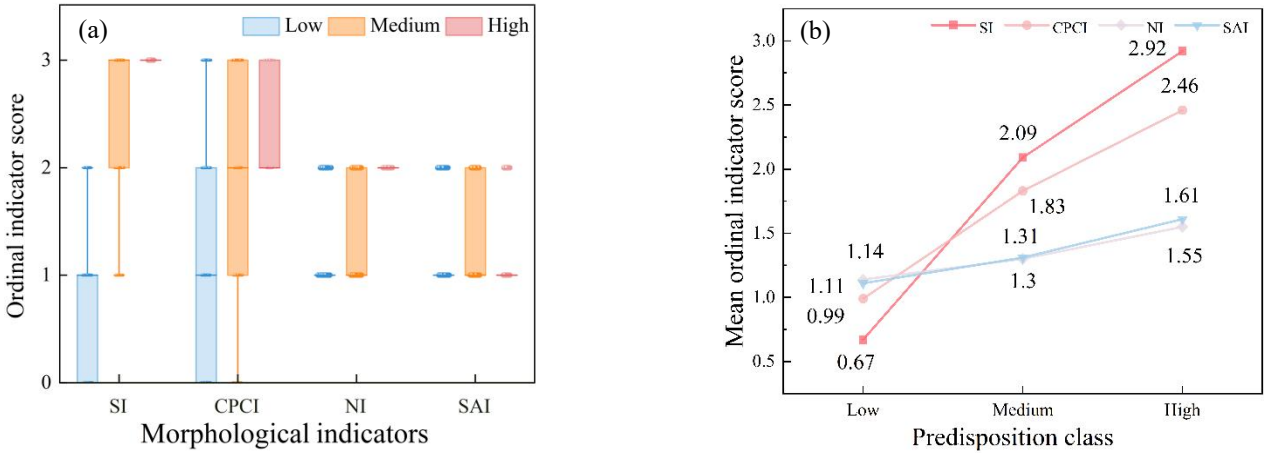


Figure 5. Distributional characteristics of the channel-morphology indicators across predisposition classes: (a) distributions of the ordinal scores of each morphological indicator within the Low, Medium, and High classes; and (b) variation in the mean ordinal scores of the morphological indicators among predisposition classes.

4.3 Comparison of ice-jam predisposition model configurations

The four configurations produced clearly different class compositions (Table 5), reflecting the information added at each modelling step. M1 contained only narrowing and sinuosity, whereas the contrast between M2 and M3 shows how SAI and CPCI supplement this baseline along different morphological dimensions. Their differences were also apparent in the historical-record comparison. M4 placed 78.7% of the records in Medium- or High-class units, compared with 76.6% for M1, 57.4% for M2, and 66.0% for M3, and it produced the smallest Low-class share (21.3%). M1, by contrast, placed the largest proportion of records in the High class (42.6%). The configurations therefore involve a trade-off between broad coverage of historical locations and concentration within the High class. Because the present study is intended for regional screening, M4 was selected for the subsequent spatial analysis to reduce the likelihood that morphologically complex reaches would remain in the Low class. This choice reflects the screening objective and should not be interpreted as evidence that M4 is more predictively accurate than M1.

Table 5. Ice-jam predisposition class composition under the different model configurations.

Model	Low count	Medium count	High count	Low (%)	Medium (%)	High (%)
M1	686	677	207	43.69	43.12	13.18
M2	858	598	114	54.65	38.09	7.26
M3	697	649	224	44.39	41.34	14.27
M4	758	626	186	48.28	39.87	11.85

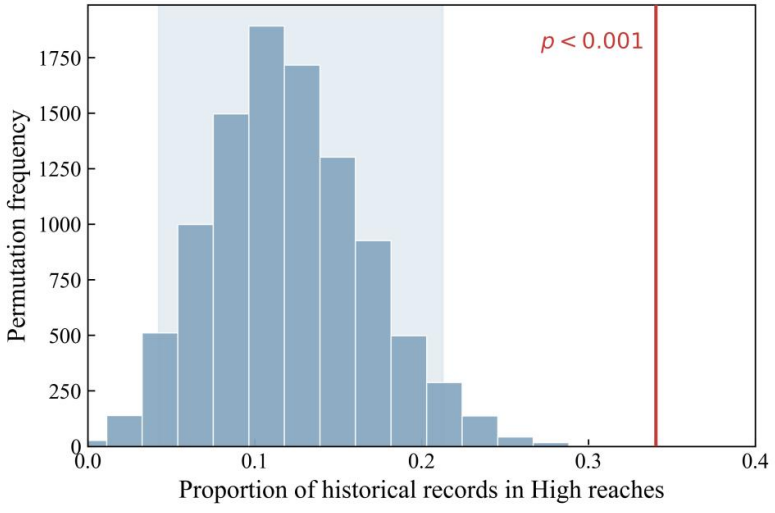
https://doi.org/10.5194/egusphere-2026-6258
Preprint. Discussion started: 3 November 2026
© Author(s) 2026. CC BY 4.0 License.

The enrichment ratio provides further context for this trade-off because it evaluates High-class coverage relative to the prevalence of the High class itself (Table 6). M2 produced a relatively high ratio, showing that its historical locations were concentrated within a small High-class extent; however, only 57.4% of the records fell in its Medium and High classes combined. M4 retained substantial enrichment while increasing this combined coverage to 78.7%. Thus, M2 provided a more concentrated High-class signal, whereas M4 represented a broader set of potentially predisposed reaches under complex channel conditions.

Table 6. Spatial consistency between historical ice-jam records and the predisposition classes produced by different model configurations.

Model	Low	Medium	High	Medium-High	High-class enrichment ratio (ER)
M1	23.4%	34.0%	42.6%	76.6%	3.23
M2	42.6%	31.9%	25.5%	57.4%	3.52
M3	34.0%	38.3%	27.7%	66.0%	1.94
M4	21.3%	44.7%	34.0%	78.7%	2.87

The permutation test confirmed that the High-class concentration under M4 was unlikely to arise from random allocation (Fig. 6). Although only 11.85% of the 500 m units were classified as High, these units contained 16 of the 47 historical locations (34.0%), yielding an enrichment ratio of 2.87. Random reassignment produced a mean of 5.56 locations in the High class and a 95% interval of 2-10. The observed count of 16 exceeded this distribution ($p < 0.001$), indicating significant spatial concentration of historical ice-jam locations within the High-class units identified by M4.



https://doi.org/10.5194/egusphere-2026-6258
Preprint. Discussion started: 3 November 2026
© Author(s) 2026. CC BY 4.0 License.

Figure 6. Random permutation distribution of the proportion of historical ice-jam locations falling within reaches classified as High under M4. The red line indicates the observed proportion (34.0 %), the shaded band denotes the 95 % permutation interval, and the histogram shows the results of 9,999 random permutations.

4.4 Spatial distribution of ice-jam predisposition

At the 500 m scale, M4 classified 48.28% of the assessment units as Low, 39.87% as Medium, and 11.85% as High (Fig. 7). The dominance of the Low and Medium classes indicates that most of the study reach has comparatively low to moderate morphological predisposition. High-class units form a much smaller component and are therefore concentrated in a limited number of local sections rather than distributed throughout the river.

This concentration is also evident in the longitudinal pattern. High-class units generally occur as short contiguous sections or isolated patches, often embedded within longer Low- or Medium-class reaches, rather than forming an extensive continuous zone. Ice-jam predisposition therefore does not change monotonically from upstream to downstream; instead, local variations in channel morphology interrupt the broader pattern. The more extensive Low and Medium classes consequently provide the regional background against which the local High-class reaches stand out.

Because of this localised pattern, upstream-downstream position alone is insufficient for identifying highly predisposed reaches. Their delineation instead requires the combined interpretation of several morphological characteristics. The subsequent analysis therefore first aggregated the 500 m units into hydrological control reaches to examine broader longitudinal differences and then selected representative High-class reaches to investigate the local indicator combinations underlying those differences.

https://doi.org/10.5194/egusphere-2026-6258
Preprint. Discussion started: 3 November 2026
© Author(s) 2026. CC BY 4.0 License.

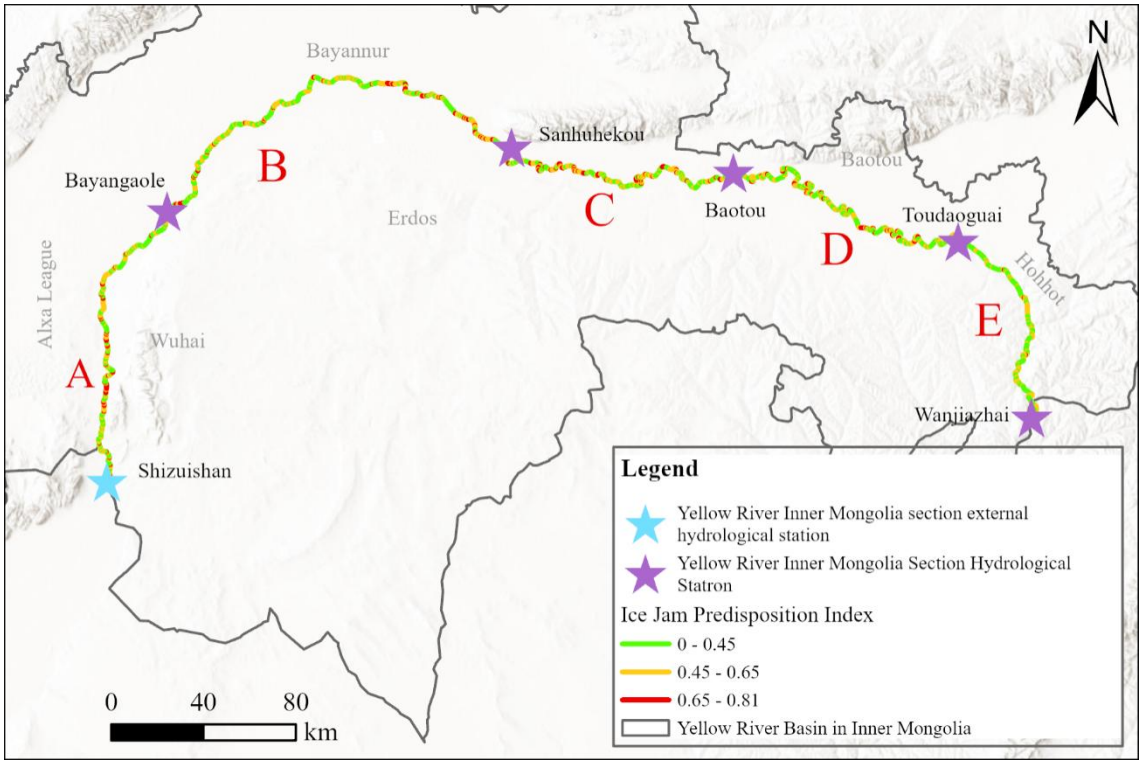
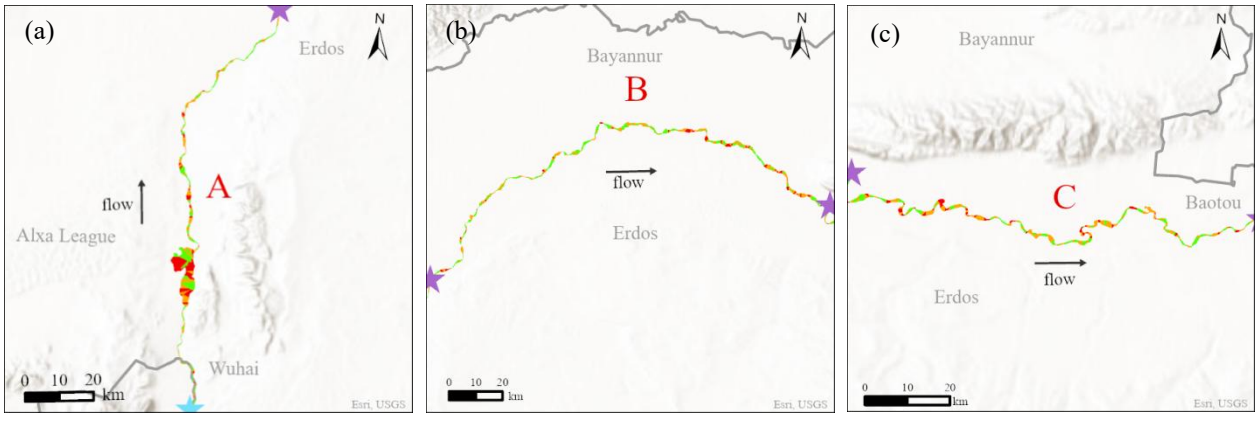


Figure 7. Spatial distribution of ice-jam predisposition under M4 at an assessment-unit length of 500 m.

4.5 Hydrological control reaches and representative High-class reaches

Grouping the 500 m units by hydrological control station revealed clear longitudinal contrasts among Reaches A-E (Fig. 8). Reach C had both the highest mean IJPI and the strongest concentration of High-class units, whereas Reach E had the lowest overall predisposition under its prevailing morphology. Reaches A, B, and D occupied intermediate positions. This ordered contrast shows that predisposition varies among hydrological control reaches rather than being distributed uniformly along the Inner Mongolia main stem.



https://doi.org/10.5194/egusphere-2026-6258
Preprint. Discussion started: 3 November 2026
© Author(s) 2026. CC BY 4.0 License.

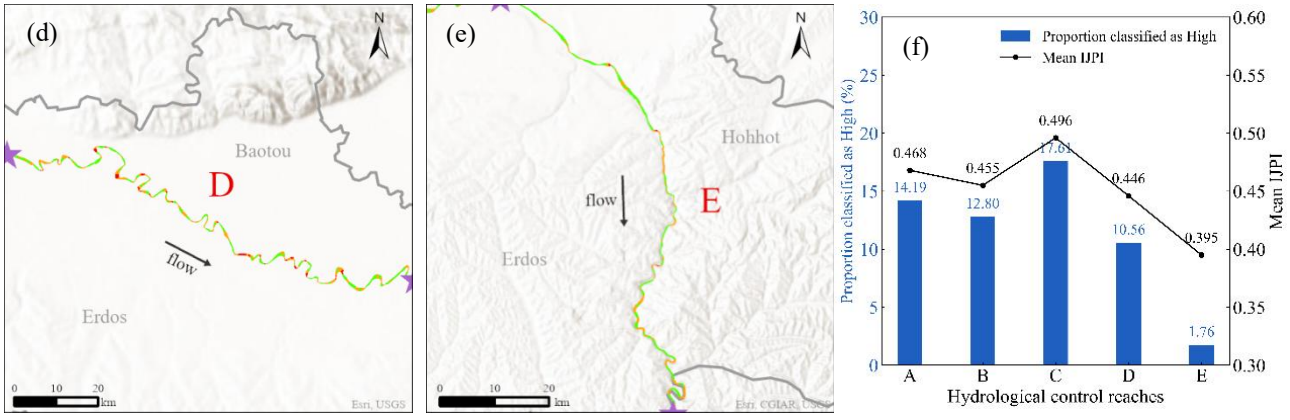
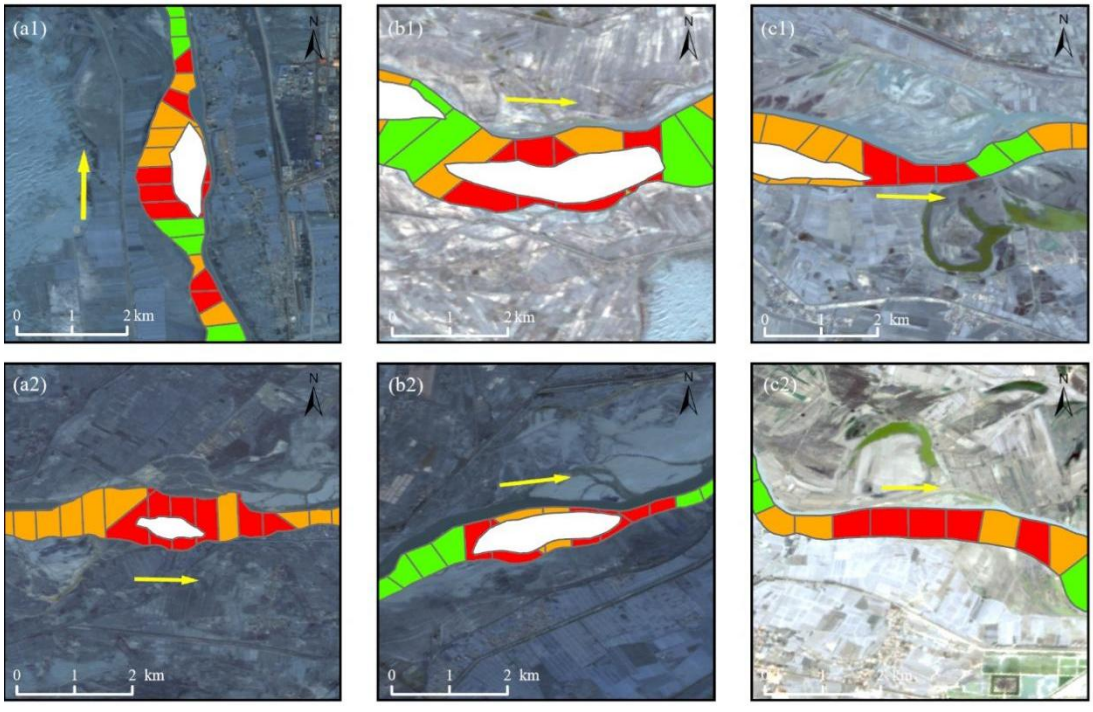


Figure 8. Spatial distribution and predisposition statistics of hydrological control reaches A–E. Panels (a)–(e) show the five longitudinal reaches delineated according to the locations of the hydrological control stations; the colours indicate the ice-jam predisposition classes of the 500 m assessment units under M4. Panel (f) shows the proportion of units classified as High and the mean IJPI for each hydrological control reach.

The reach-level comparison was followed by a local analysis of representative High-class sections (Fig. 9). Selection considered three features together: IJPI class, the dominant indicator combination, and the continuity of neighbouring High-class units. This procedure ensured that the selected sections represented distinct morphological settings rather than isolated high values. On the basis of their SI, CPCI, SAI, and NI combinations, they were grouped into three descriptive types: the bending-planform complexity type, the bending-bar-channel complexity type, and the bending-local confinement type.



https://doi.org/10.5194/egusphere-2026-6258
Preprint. Discussion started: 3 November 2026
© Author(s) 2026. CC BY 4.0 License.

Figure 9. Channel-morphology characteristics of representative highly predisposed reaches. Panels (a1) and (a2) show reaches of the bending-planform complexity type, panels (b1) and (b2) show reaches of the bending-bar-channel complexity type, and panels (c1) and (c2) show reaches of the bending-local confinement type.

The three types share high sinuosity but differ in the factor accompanying it. Reaches of the bending-planform complexity type combine high SI and CPCI scores and exhibit irregular boundaries and complex bar-channel configurations. Reaches of the bending-bar-channel complexity type instead combine high SI and SAI, indicating a large shoal proportion and a pronounced association between the main channel and shoals. In reaches of the bending-local confinement type, high SI occurs together with high NI, so bending and narrowing jointly increase channel confinement. Although all three types have high IJPI values, their contrasting indicator combinations show that no single morphology defines the High class. Rather, planform complexity, shoal development, and local narrowing provide alternative pathways to an elevated composite classification within a generally sinuous setting (Table 7).

Table 7. Morphological indicator characteristics of representative highly predisposed reaches.

Typical reach type	SI class	CPCI class	SAI class	NI class	Mean IJPI
Bending-planform complexity type	3.00	3.00	1.92	1.17	0.700
Bending-bar-channel complexity type	3.00	2.00	2.00	2.00	0.771
Bending-local confinement type	3.00	1.66	1.00	2.00	0.750

4.6 Weight-sensitivity analysis

Weight sensitivity was assessed using six weighting schemes for M4 (Table 8). These included the baseline scheme W0 and five alternative schemes, W1–W5. The alternative schemes changed the weights of NI, SI, SAI, and CPCI. All six schemes used the same input data and class thresholds. This ensured that differences among schemes reflected changes in weights.

Table 8. Sensitivity analysis of the ice-jam predisposition assessment results under different weighting schemes.

Weight scenario	NI	SI	SAI	CPCI	Spearman ρ	Agreement	ER
W0	0.400	0.250	0.200	0.150	—	—	2.87
W1	0.462	0.288	0.143	0.107	0.974	88.2%	2.52
W2	0.338	0.212	0.257	0.193	0.976	92.3%	1.34
W3	0.400	0.250	0.175	0.175	0.999	99.8%	1.46
W4	0.400	0.250	0.150	0.200	0.996	99.6%	1.31
W5	0.250	0.250	0.250	0.250	0.962	84.8%	0.96

Across the tested scenarios, continuous IJPI values remained closely aligned with the W0 baseline (Table 8). Spearman rank correlations exceeded 0.96 in every case, indicating that the relative ordering of reaches changed little as the weights varied. This stability was strongest for W3 and W4, which altered the relative contributions of SAI and CPCI: their correlations with

https://doi.org/10.5194/egusphere-2026-6258
Preprint. Discussion started: 3 November 2026
© Author(s) 2026. CC BY 4.0 License.

W0 were 0.999 and 0.996, and their class-agreement rates were 99.8% and 99.6%, respectively. Moderate changes in the balance between the two newly introduced indicators therefore had little effect on the principal highly predisposed reaches. Class assignments were somewhat more sensitive than the continuous rankings, but agreement remained high for every scenario except W5. Under W5, assigning equal weights to all four indicators reduced agreement with the baseline to 84.8%, showing that equal weighting changed a meaningful number of classifications. W1 and W2 also altered the balance between conventional and newly introduced indicators, yet their spatial correlation with W0 remained strong. The model is therefore stable within the tested range of non-equal weights, although the equal-weight case demonstrates that the indicators cannot be treated as interchangeable without affecting the resulting classes.

The historical-record comparison adds a second perspective on this sensitivity. All scenarios captured at least some areas in which historical events were concentrated, but W1 produced the highest High-class enrichment ratio among the alternatives (ER = 2.52). Increasing the relative contributions of NI and SI was therefore associated with stronger concentration of historical locations in the High class. By contrast, W2, W3, and W4 remained close to W0 in continuous IJPI and class assignment even though their enrichment ratios and significance levels differed. Weight variation thus had little effect on the broad High-class pattern but did affect how closely the final class boundary corresponded to the historical locations.

5 Discussion

5.1 Role of multi-channel morphology in the predisposition assessment

Existing geospatial assessments generally identify reaches with restricted ice transport from channel narrowing, sinuosity, and local obstructions (De Munck et al., 2017; Kalinin, 2008). These variables capture the overall geometry of the main channel, but they do not distinguish all internal configurations found along the Inner Mongolia reach, where dense shoals, extensive branching, and complex bar-channel boundaries are common. Consequently, reaches with similar width and sinuosity can still differ substantially in the arrangement of flow pathways and exposed bars. Adding SAI and CPCI addresses this limitation by separating the extent of shoal development from the complexity of its spatial organisation. This distinction is consistent with multi-channel river morphology, in which the main channel, shoals, and branching channels jointly define the overall planform (Ashmore, 2013; Church, 2006; Williams et al., 2016).

The internal morphology represented by SAI and CPCI may also have hydraulic implications. Shoals and branching can redistribute discharge, alter local conveyance and velocity, and redirect ice-transport pathways, potentially favouring retention in low-velocity zones or at junctions between main and secondary channels (Nafziger et al., 2019; Osada et al., 2020). The two indices therefore extend the assessment beyond overall width and sinuosity and help distinguish reaches with similar external geometry but different internal structure. These links remain process-based interpretations rather than direct model outputs, however, because the present study did not simulate flow or ice movement. They should consequently be tested with hydrological, ice-regime, and hydrodynamic data.

https://doi.org/10.5194/egusphere-2026-6258
Preprint. Discussion started: 3 November 2026
© Author(s) 2026. CC BY 4.0 License.

The comparison between M1 and M4 illustrates how the intended application affects model choice. M1 emphasises narrowing and sinuosity and concentrates a relatively large share of historical locations in the High class. M4, after adding shoal development and planform complexity, instead provides the highest combined Medium- and High-class coverage and the smallest Low-class share. The two configurations therefore favour different outcomes: a more concentrated High-class signal under M1 and broader regional screening under M4. Because the present objective is to avoid overlooking morphologically complex reaches along a long river corridor, M4 was used for the subsequent spatial analysis. This application-based choice does not demonstrate greater predictive accuracy.

SAI and CPCI are correlated because both draw on shoal information, but the sensitivity analysis shows that their contributions are not identical. Across alternative weights, the continuous IJPI rankings and broad spatial pattern remained strongly aligned with the baseline, indicating that the main longitudinal contrasts are comparatively robust. The exact High-class extent and the enrichment ratio nevertheless changed among scenarios. Robustness should therefore be understood as stability in relative ranking and overall pattern, not as invariance in class boundaries or historical-location statistics.

5.2 Morphological combinations and spatial differences among highly predisposed reaches

The representative High-class reaches show that high predisposition can arise from several morphological combinations. High SI is common to all three types, but it is paired with high CPCI, high SAI, or high NI depending on the reach. Sinuosity may therefore provide a shared morphological setting, while planform complexity, shoal development, and local narrowing differentiate the local pathways to a high composite score. This interpretation is consistent with previous studies linking ice-jam locations to bends and changes in channel width (Beltaos, 2008; Shen, 2010; Zhao et al., 2021). The three types nevertheless have similar mean IJPI values of 0.700-0.771, demonstrating that comparable composite predisposition can result from different indicator combinations. Their identification should therefore be used to interpret within-study variation rather than as a universal classification of river types.

The permutation test supports the spatial relevance of this classification but does not establish the physical role of each combination. Historical locations occurred in High-class units more often than expected under random allocation ($p < 0.001$), demonstrating non-random correspondence between the modelled pattern and the event record. This result strengthens the interpretation that the High class captures meaningful spatial differences, but it cannot separate the effects of sinuosity, shoal development, complexity, and narrowing during individual events. Positional uncertainty in the historical records and the temporal mismatch with the imagery further limit any process-based inference.

5.3 Effects of assessment scale on the spatial representation of ice-jam predisposition

The scale analysis separates regional stability from local positional uncertainty. Overall class composition changed little among the 250, 500, and 1000 m units, but the locations of individual High-class reaches changed markedly. Short units preserve local variation but are sensitive to the segmentation origin, unit boundaries, and short-distance anomalies; long units improve continuity but can average local high values with adjacent reaches. Differences among scales therefore arise mainly

https://doi.org/10.5194/egusphere-2026-6258
Preprint. Discussion started: 3 November 2026
© Author(s) 2026. CC BY 4.0 License.

from the changing extent of spatial aggregation. Comparable effects are reported in landscape-pattern analysis and susceptibility mapping (Reichenbach et al., 2018; Wu et al., 2002). On balance, the 500 m unit provided a workable compromise for this dataset, although it should not be regarded as universally optimal.

Reaches classified as High at all three scales provide a comparatively stable subset for priority investigation because their identification is less dependent on a single segmentation length. This cross-scale agreement has a limited interpretation: it indicates persistence under different aggregation extents, not a probability of ice-jam occurrence or temporal stability. Likewise, the choice of 500 m reflects the resolution and channel conditions of the present study. Applications elsewhere should reconsider the scale in relation to channel width, the spatial extent of morphological change, and the purpose of the assessment.

5.4 Study limitations and directions for future improvement

The IJPI is intended as a preliminary screening tool for long river reaches where continuous ice and hydrodynamic observations are unavailable. In that role, it can delineate candidate areas for remote-sensing interpretation, field inspection, and monitoring-site deployment. Management decisions should then combine these candidates with historical ice conditions, hydrological processes, and the distribution of protected assets. The framework therefore represents relative predisposition associated with channel morphology; it does not predict the timing of an event or the magnitude of ice-jam-induced backwater.

The first major source of uncertainty is the temporal mismatch among the datasets. Historical events were recorded in 1991-2005, whereas the morphological indicators describe conditions visible in 2025. Because the study reach undergoes erosion, deposition, main-channel migration, and changes in shoal morphology, the analysis can establish only spatial correspondence between historical locations and present-day morphology, not contemporaneous validation. Differences in water level among the four satellite scenes introduce an additional uncertainty because they may alter mapped shoal boundaries and hence SAI and CPCI. Multi-year imagery acquired under comparable water-level conditions would help determine whether high-IJPI reaches persist or shift as the channel adjusts.

A second source of uncertainty concerns event location. Some historical records identify only a nearby village, bridge, or river reach, so their assessment units were inferred from place names and upstream-downstream relationships. Keeping the IJPI layer hidden during geolocation reduced the risk of model-informed assignment, but it could not eliminate positional error. Future validation would therefore benefit from an event database containing occurrence time, spatial extent, positional accuracy, and ice-regime characteristics, together with records from independent years or new observations. More generally, static morphology represents only one part of the setting in which ice jams form (Beltaos and Prowse, 2009). Air temperature, discharge, water level, ice thickness, ice concentration, and reservoir operation jointly determine whether and how a jam develops (Fu et al., 2014; Su et al., 2019). Combining multi-temporal morphology, field ice observations, and hydrodynamic modelling would extend the present spatial screening towards event-specific process analysis.

https://doi.org/10.5194/egusphere-2026-6258
Preprint. Discussion started: 3 November 2026
© Author(s) 2026. CC BY 4.0 License.

6 Conclusions

This study developed a spatial ice-jam predisposition framework that integrates channel narrowing, sinuosity, shoal development, and channel planform complexity along the Inner Mongolia reach of the Yellow River. At the 500 m scale, M4 classified 48.28%, 39.87%, and 11.85% of the assessment units as Low, Medium, and High, respectively. The High class was locally concentrated in sinuous reaches where planform complexity, shoal development, or local narrowing provided additional morphological constraints. These combinations produced three descriptive types: the bending-planform complexity type, the bending-bar-channel complexity type, and the bending-local confinement type, with mean IJPI values of 0.700-0.771. Although assessment scale had little effect on overall class composition, it affected the locations of individual High-class reaches. Historical records nevertheless showed non-random spatial correspondence with the M4 pattern: 78.7% fell within Medium- or High-class units, and the High-class count exceeded random expectation.

Taken together, the results show that the IJPI can support preliminary regional screening of ice-jam-prone reaches and provide a spatial basis for field inspection, monitoring-site deployment, and priority-reach identification. Its interpretation should remain limited to relative predisposition under the observed channel-morphology conditions because dynam`ic controls such as air temperature, discharge, ice evolution, and reservoir regulation are not included. Integrating multi-temporal remote sensing, long-term ice records, and hydrodynamic modelling would improve the temporal relevance of the framework and provide stronger support for process-based interpretation.

Code and data availability

The raw data supporting the conclusions of this article will be made available by the authors on request.

Author contributions

XS: Conceptualisation, Data collection and curation, Analysis, Methodology, Software, Validation, Visualisation, Writing–original draft, review and editing. HJ: Conceptualisation, Funding acquisition, Methodology, Project administration. HL: Supervision, Validation, Writing–review and editing. ZX: Data collection and curation, Analysis, Validation, Writing–review and editing. ZC: Data collection and curation, Visualisation, Writing–review and editing.

Competing interests

The contact author has declared that none of the authors has any competing interests.

https://doi.org/10.5194/egusphere-2026-6258
Preprint. Discussion started: 3 November 2026
© Author(s) 2026. CC BY 4.0 License.

Disclaimer

Publisher's note: Copernicus Publications remains neutral with regard to jurisdictional claims made in the text, published maps, institutional affiliations, or any other geographical representation in this paper. While Copernicus Publications makes every effort to include appropriate place names, the final responsibility lies with the authors. Views expressed in the text are those of the authors and do not necessarily reflect the views of the publisher.

Acknowledgements

The authors would like to thank the Editor and the anonymous reviewers for their constructive comments and suggestions on earlier versions of the manuscript, which helped improve the clarity and quality of this work.

Financial support

This research was funded by the National Natural Science Foundation of China (Grant No. 52379014), the Joint Fund of the National Natural Science Foundation of China (Grant No. U23A2012), the Inner Mongolia Key Fund for Natural Sciences (Grant No. 2026ZD028), and the 2025 Science and Technology Support Project of State Key Laboratory of Water Engineering Ecology and Environment in Arid Area (Grant No. 2025GJCXPT01005).

References

Arnone, E., Francipane, A., Scarbaci, A., Puglisi, C., and Noto, L. V.: Effect of raster resolution and polygon-conversion algorithm on landslide susceptibility mapping, Environmental Modelling & Software, 84, 467–481, https://doi.org/10.1016/j.envsoft.2016.07.016, 2016.

Arsenault-Boucher, L., Boucher, É., Lhissou, R., Chokmani, K., and Kinnard, C.: Addressing Biases in Ice Jam Observations by Integrating Multi-Source Data in a Forested Fluvial Landscape, Southern Quebec, River Research & Apps, 42, 1188–1208, https://doi.org/10.1002/rra.70133, 2026.

Ashmore, P.: 9.17 Morphology and Dynamics of Braided Rivers, in: Treatise on Geomorphology, Elsevier, 289–312, https://doi.org/10.1016/B978-0-12-374739-6.00242-6, 2013.

Ashmore, P. E.: How do gravel-bed rivers braid?, Can. J. Earth Sci., 28, 326–341, https://doi.org/10.1139/e91-030, 1991.

Bai T., Yang Y., Wu C., Zhao X., and Wang Z.: Theory and Practice of Ice-Flood Control Operations in the Ningxia–Inner Mongolia Reach of the Yellow River, China Water & Power Press, Beijing, China, 243 pp., https://lib.kmu.edu.cn/info/1101/7678.htm (last access: 29 October 2026), 2021.

Beltaos, S.: Progress in the study and management of river ice jams, Cold Regions Science and Technology, 51, 2–19, https://doi.org/10.1016/j.coldregions.2007.09.001, 2008.

https://doi.org/10.5194/egusphere-2026-6258
Preprint. Discussion started: 3 November 2026
© Author(s) 2026. CC BY 4.0 License.

Beltaos, S. and Prowse, T.: River-ice hydrology in a shrinking cryosphere, Hydrological Processes, 23, 122–144, https://doi.org/10.1002/hyp.7165, 2009.

Beltaos, S. and Prowse, T. D.: Climate impacts on extreme ice-jam events in Canadian rivers, Hydrological Sciences Journal, 46, 157–181, https://doi.org/10.1080/02626660109492807, 2001.

Beltaos, S., Ismail, S., and Burrell, B. C.: Midwinter breakup and jamming on the upper Saint John River: a case study, Can. J. Civ. Eng., 30, 77–88, https://doi.org/10.1139/l02-062, 2003.

Beltaos, S., Miller, L., Burrell, B. C., and Sullivan, D.: Formation of Breakup Ice Jams at Bridges, J. Hydraul. Eng., 132, 1229–1236, https://doi.org/10.1061/(ASCE)0733-9429(2006)132:11(1229), 2006.

Chu, T. and Lindenschmidt, K.-E.: Effects of River Geomorphology on River Ice Freeze-up and Break-up Rates Using MODIS Imagery, Canadian Journal of Remote Sensing, 45, 176–191, https://doi.org/10.1080/07038992.2019.1635004, 2019.

Church, M.: Bed material transport and the morphology of alluvial river channels, Annu. Rev. Earth Planet. Sci., 34, 325–354, https://doi.org/10.1146/annurev.earth.33.092203.122721, 2006.

De Munck, S., Gauthier, Y., Bernier, M., Chokmani, K., and Légaré, S.: River predisposition to ice jams: a simplified geospatial model, Nat. Hazards Earth Syst. Sci., 17, 1033–1045, https://doi.org/10.5194/nhess-17-1033-2017, 2017.

Ettema, R. and Muste, M.: Laboratory Observations of Ice Jams in Channel Confluences, J. Cold Reg. Eng., 15, 34–58, https://doi.org/10.1061/(ASCE)0887-381X(2001)15:1(34), 2001.

Ettema, R. and Zabilansky, L.: Ice Influences on Channel Stability: Insights from Missouri's Fort Peck Reach, J. Hydraul. Eng., 130, 279–292, https://doi.org/10.1061/(ASCE)0733-9429(2004)130:4(279), 2004.

Frasson, R. P. D. M., Wei, R., Durand, M., Minear, J. T., Domeneghetti, A., Schumann, G., Williams, B. A., Rodriguez, E., Picamilh, C., Lion, C., Pavelsky, T., and Garambois, P.-A.: Automated River Reach Definition Strategies: Applications for the Surface Water and Ocean Topography Mission, Water Resources Research, 53, 8164–8186, https://doi.org/10.1002/2017WR020887, 2017.

Fu, C., Popescu, I., Wang, C., Mynett, A. E., and Zhang, F.: Challenges in modelling river flow and ice regime on the Ningxia–Inner Mongolia reach of the Yellow River, China, Hydrol. Earth Syst. Sci., 18, 1225–1237, https://doi.org/10.5194/hess-18-1225-2014, 2014.

Gauthier, Y., Paquet, L.-M., Gonzalez, A., and Bernier, M.: Using Radar Images and Gis to Support ICE-Related Flood Forecasting/Utilisation D'ImagesRadar ET D'un Sig En Appui À La Prévision Des Crues Hivernales, Geomatica, 62, 139–149, https://doi.org/10.5623/geomat-2008-0018, 2008.

Hicks, F.: An overview of river ice problems: CRIPE07 guest editorial, Cold Regions Science and Technology, 55, 175–185, https://doi.org/10.1016/j.coldregions.2008.09.006, 2009.

IAHR Working Group on River Ice Hydraulics: River Ice Jams; a State-of-the-Art Report, in: Proceedings of the 8th IAHR International Symposium on Ice, Iowa City, USA, III, 561–594,https://www.iahr.org/library/infor?pid=28407 (last access: 29 October 2026), 1986.

Jelinski, D. E. and Wu, J.: The modifiable areal unit problem and implications for landscape ecology, Landscape Ecol, 11, 129–140, https://doi.org/10.1007/BF02447512, 1996.

https://doi.org/10.5194/egusphere-2026-6258
Preprint. Discussion started: 3 November 2026
© Author(s) 2026. CC BY 4.0 License.

Kalinin, V. G.: Study of spatial distribution and occurrence frequency of ice jams in rivers of the Votkinsk reservoir catchment, Russ. Meteorol. Hydrol., 33, 819–822, https://doi.org/10.3103/S1068373908120091, 2008.

Kong, G., Bai, T., Chang, J., Wu, C., and Liu, D.: Flow routing during ice control period, Water Resour, 42, 627–634, https://doi.org/10.1134/S0097807815050048, 2015.

Kovachis, N., Burrell, B. C., Huokuna, M., Beltaos, S., Turcotte, B., and Jasek, M.: Ice-jam flood delineation: Challenges and research needs, Canadian Water Resources Journal / Revue canadienne des ressources hydriques, 42, 258–268, https://doi.org/10.1080/07011784.2017.1294998, 2017.

Li, C., Dai, J., Leng, Y., Hao, X., Li, W., Akmalov, S., Li, X., Wang, Z., Gao, H., Fu, X., Hu, S., and Zheng, Y.: Characterization of Local and Long-Distance Ice Floe Motion in the Yellow River Using UAV–GPS Joint Observations, Remote Sensing, 18, 823, https://doi.org/10.3390/rs18050823, 2026.

Lindenschmidt, K.-E.: RIVICE—A Non-Proprietary, Open-Source, One-Dimensional River-Ice Model, Water, 9, 314, https://doi.org/10.3390/w9050314, 2017.

Lindenschmidt, K.-E., Rokaya, P., Das, A., Li, Z., and Richard, D.: A novel stochastic modelling approach for operational real-time ice-jam flood forecasting, Journal of Hydrology, 575, 381–394, https://doi.org/10.1016/j.jhydrol.2019.05.048, 2019.

Lindenschmidt, K.-E., Briggs, R., Khan, A. A., and Puestow, T.: Requirements for the Development and Operation of a Freeze-Up Ice-Jam Flood Forecasting System, Water, 16, 2648, https://doi.org/10.3390/w16182648, 2024.

Madaeni, F., Lhissou, R., Chokmani, K., Raymond, S., and Gauthier, Y.: Ice jam formation, breakup and prediction methods based on hydroclimatic data using artificial intelligence: A review, Cold Regions Science and Technology, 174, 103032, https://doi.org/10.1016/j.coldregions.2020.103032, 2020.

Murray, A. B. and Paola, C.: A cellular model of braided rivers, Nature, 371, 54–57, https://doi.org/10.1038/371054a0, 1994.

Nafziger, J., She, Y., and Hicks, F.: Dynamic river ice processes in a river delta network, Cold Regions Science and Technology, 158, 275–287, https://doi.org/10.1016/j.coldregions.2018.09.005, 2019.

Osada, K., Ettema, R., Shimizu, Y., and Wakai, A.: Influence of Channel Morphology on Ice Conveyance and Bridging: Experiments with a Numerical Model, J. Cold Reg. Eng., 34, 04019017, https://doi.org/10.1061/(ASCE)CR.1943-5495.0000201, 2020.

Prowse, T., Shrestha, R., Bonsal, B., and Dibike, Y.: Changing spring air-temperature gradients along large northern rivers: Implications for severity of river-ice floods, Geophysical Research Letters, 37, L19706, https://doi.org/10.1029/2010GL044878, 2010.

Prowse, T. D.: River-Ice Ecology. I: Hydrologic, Geomorphic, and Water-Quality Aspects, J. Cold Reg. Eng., 15, 1–16, https://doi.org/10.1061/(ASCE)0887-381X(2001)15:1(1), 2001.

Prowse, T. D. and Beltaos, S.: Climatic control of river-ice hydrology: a review, Hydrological Processes, 16, 805–822, https://doi.org/10.1002/hyp.369, 2002.

Reichenbach, P., Rossi, M., Malamud, B. D., Mihir, M., and Guzzetti, F.: A review of statistically-based landslide susceptibility models, Earth-Science Reviews, 180, 60–91, https://doi.org/10.1016/j.earscirev.2018.03.001, 2018.

https://doi.org/10.5194/egusphere-2026-6258
Preprint. Discussion started: 3 November 2026
© Author(s) 2026. CC BY 4.0 License.



Saisana, M., Saltelli, A., and Tarantola, S.: Uncertainty and Sensitivity Analysis Techniques as Tools for the Quality Assessment of Composite Indicators, Journal of the Royal Statistical Society Series A: Statistics in Society, 168, 307–323, https://doi.org/10.1111/j.1467-985X.2005.00350.x, 2005.

Shen, H. T.: Mathematical modeling of river ice processes, Cold Regions Science and Technology, 62, 3–13, https://doi.org/10.1016/j.coldregions.2010.02.007, 2010.

Shirzadi, A., Solaimani, K., Roshan, M. H., Kavian, A., Chapi, K., Shahabi, H., Keesstra, S., Ahmad, B. B., and Bui, D. T.: Uncertainties of prediction accuracy in shallow landslide modeling: Sample size and raster resolution, CATENA, 178, 172–188, https://doi.org/10.1016/j.catena.2019.03.017, 2019.

Su, T., Huang, H., Zhou, Y., and Yu, G.: Dam Operation for Mitigating Ice Jam Flooding Risks under the Adjustment of River Channel-Forms: Implications from an Evaluation in the Ningxia-Inner Mongolia Reach of the Upper Yellow River, China, Water, 11, 1136, https://doi.org/10.3390/w11061136, 2019.

Turner, M. G., O'Neill, R. V., Gardner, R. H., and Milne, B. T.: Effects of changing spatial scale on the analysis of landscape pattern, Landscape Ecol, 3, 153–162, https://doi.org/10.1007/BF00131534, 1989.

Unterschultz, K. D., Van Der Sanden, J., and Hicks, F. E.: Potential of RADARSAT-1 for the monitoring of river ice: Results of a case study on the Athabasca River at Fort McMurray, Canada, Cold Regions Science and Technology, 55, 238–248, https://doi.org/10.1016/j.coldregions.2008.02.003, 2009.

Wan, Z., Shi, H., Liu, X., and Liu, H.: Analysis on the Ice Regime Change Characteristics in the Inner Mongolia Reach of the Yellow River from 1950 to 2010, Journal of Coastal Research, 115, 405-408, https://doi.org/10.2112/JCR-SI115-115.1, 2020.

Williams, R. D., Brasington, J., and Hicks, D. M.: Numerical Modelling of Braided River Morphodynamics: Review and Future Challenges, Geography Compass, 10, 102–127, https://doi.org/10.1111/gec3.12260, 2016.

Wu, J., Shen, W., Sun, W., and Tueller, P. T.: Empirical patterns of the effects of changing scale on landscape metrics, Landscape Ecol, 17, 761–782, https://doi.org/10.1023/A:1022995922992, 2002.

Zhao, S.-X., Wang, W.-J., Shi, X.-H., Zhao, S.-N., Wu, Y.-J., Quan, Q., Li, C., Szydlowski, M., Li, W., and Kolerski, T.: Freeze-Up Ice Jam Formation in the River Bend, a Case Study on the Inner Mongolia Reach of Yellow River, Crystals, 11, 631, https://doi.org/10.3390/cryst11060631, 2021.